Vertical organic spin valves in perpendicular magnetic fields

M. Grünewald,[1,2] R. Göckeritz,[2] N. Homonnay,[2] F. Würthner,[3,4] L. W. Molenkamp,[1,3] and G. Schmidt[1,2,*]
[1]Physikalisches Institut (EP3), Universität Würzburg, Am Hubland, D-97074 Würzburg, Germany
[2]Institute of Physics, Martin-Luther-Universität Halle-Wittenberg, Von-Danckelmann-Platz 3, D-06120 Halle, Germany
[3]Röntgen Center for Complex Material Systems, Universität Würzburg, Am Hubland, D-97074 Würzburg, Germany
[4]Institut für Organische Chemie, Universität Würzburg, Am Hubland, D-97074 Würzburg, Germany
(Received 22 April 2013; published 26 August 2013)

We report the results of magnetoresistance measurements in vertical organic spin valves with the magnetic field oriented perpendicular to the layer stack. The magnetoresistance measurements were performed after carefully preparing either parallel or antiparallel in-plane magnetization states of the magnetic electrodes in order to observe traces of Hanle precession. Due to the low mobility in organic semiconductors, the transit time of spin-polarized carriers should allow for precession of the spins in perpendicular fields which in statistical average would quench the magnetoresistance. However, in none of the experiments do we observe any change in resistance while sweeping the perpendicular field, up to the point where the electrode's magnetization starts to reorient. This absence of Hanle-type effects indicates that the magnetoresistance is not based on the injection of spin-polarized electrons into the organic semiconductor but rather on tunneling through pinholes superimposed with tunneling anisotropic magnetoresistance. These measurements suggest that even for clear spin-valve signatures, control experiments should be established which can confirm or disprove the electrical detection of injected spin-polarized carriers, similar to the Hanle precession in inorganic spin valves.

DOI: 10.1103/PhysRevB.88.085319 PACS number(s): 81.05.Fb, 72.25.−b, 75.76.+j

I. INTRODUCTION

A number of experiments using vertical organic spin valves (OSVs) have been demonstrated over the past years (for example, Refs. 1–8). In many cases, it is still unclear whether a tunneling-based magnetoresistance effect [tunneling magnetoresistance (TMR) or tunneling anisotropic magnetoresistance (TAMR)][6,8,9] or actual spin injection and consequently giant magnetoresistance[2,7] (GMR) is the origin of the observed effects. Although the investigation of I/V characteristics or the temperature dependence of the device resistance can give indications about the underlying transport mechanisms, final proof is still missing. Further complications arise from the facts that charge injection into organic semiconductors (OSCs) is often based on tunneling[10] and that intermixing of spin-dependent transport and TAMR (Ref. 9) can prevent a clear distinction between TMR and GMR.

In the advent of electrical spin injection into inorganic semiconductors, a similar problem existed. Especially in high mobility semiconductors, stray magnetic fields originating from magnetic contacts can modulate intrinsic magnetoresistance effects and thus mimic the signature of spin injection.[11] For electrically detected spin injection in inorganic semiconductors, the final litmus test was the investigation of Hanle precession in perpendicular magnetic fields.[12,13] It can easily be shown that the principle of Hanle precession[14,15] is also applicable for organic spin valves, although with a slightly different result.

The Hanle effect itself is based on the precession of spins with the Larmor frequency ω_L induced by a magnetic field B which is oriented perpendicular to the spin:

$$\omega_L = \frac{egB}{2m_e}, \tag{1}$$

where m_e is the electron rest mass and g the electron's g factor. Thus, the spin $\vec{s}$ (phase φ_0 at time $t = 0$) becomes time dependent and can be described by

$$\vec{s} = \frac{1}{2}\hbar \begin{pmatrix} \cos(\varphi_0 + \omega_L \cdot t) \\ \sin(\varphi_0 + \omega_L \cdot t) \end{pmatrix}. \tag{2}$$

Usually, spin-polarized transport in organic or inorganic semiconductors is demonstrated in devices consisting of a nonmagnetic transport layer placed between at least two ferromagnetic electrodes in a lateral or vertical arrangement, so-called spin-valve devices. The resistance R of a spin-valve device depends on the relative magnetization of the electrodes (antiparallel R_{AP}/parallel R_P). Provided that the electrodes exhibit different coercive fields, R therefore can be adjusted by a magnetic field B_{ip} which is applied in the sample plane.

If in a spin-valve device spins actually are injected into the nonmagnetic spacer layer and subsequently detected electrically at a second ferromagnetic electrode, the Hanle effect can cause a change of the measured signal (device resistance/current). The spins then precess in a magnetic field B_z applied perpendicular to the sample plane while the in-plane field B_{ip} is kept constant at zero. This precession changes the relative orientation of the spins with respect to the magnetization of the electrodes. This change of the spins' direction has the same consequences as a change of the electrodes' magnetization and therefore can be detected in the measured signal.

The results that can be obtained in a specific experiment investigating the presence of the Hanle effect may vary depending on the transport characteristics of the material under investigation. However, the Hanle effect always appears as spin dephasing if rather large magnetic fields B_z are applied. When B_z, which causes the spin precession, is increased ω_L also increases, i.e., the precession gets faster. If ω_L is sufficiently high, the single spins perform several full precessions during their transit through the layer under investigation. As the time t_{trans} which is needed for the transit through this layer

 ©2013 American Physical Society

can not be the same for every single spin in the material, the spin polarization of the total current averages out due to the precession. This loss of spin polarization usually is called spin dephasing.[12,16] In materials in which the spin transport occurs rather incoherently, i.e., the variation in t_{trans} is large, spin dephasing can already be observed at small B_z, resulting in a simple quenching of the magnetoresistance. In contrast, if coherent spin transport is present, large B_z must be applied in order to observe the decrease in magnetoresistance while the coherent precession is observed as so-called Hanle oscillations[13] of the resistance.

Figure 1 shows resistance traces that can be expected for measurements in perpendicular magnetic fields in a spin-valve device in which the Hanle effect is present and incoherent transport is dominating (data for the antiparallel and parallel spin-valve states are shown).

It should be noted here that in a spin valve we have to distinguish two separate phenomena, namely, the injection of spin-polarized carriers into the nonmagnetic spacer layer, which may consist of an inorganic material (metal or semiconductor) or an OSC material, and the electrical detection by a second ferromagnetic contact. In inorganic semiconductors, for example, the electrical injection of spin-polarized carriers was detected by optical means already in 1999,[17,18] while reliable electrical detection was only published in 2007.[12] Between 1999 and 2007, a number of false positives for electrical detection were found[11] and only the introduction of the Hanle effect as a robust proof could confirm that the results of Lou *et al.*[12] were really demonstrating electrical spin detection. Also, in OSCs at least two possible effects causing a spin-valve signal without the presence of electrical spin detection have been demonstrated.[9,19]

The feasibility of injection of spin-polarized carriers into OSCs has been shown in various experiments, for example,

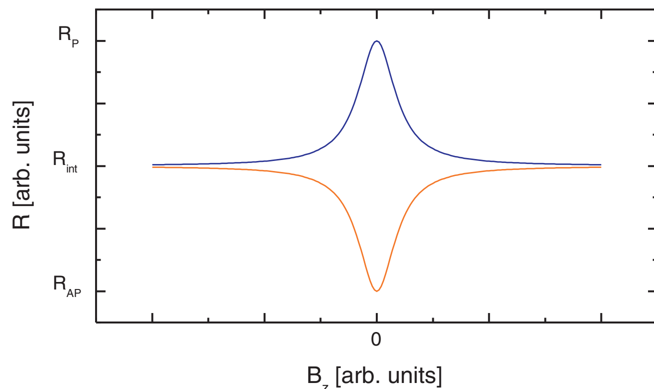

FIG. 1. (Color online) Theoretical traces of a device's resistance during experiments in a perpendicular magnetic field B_z for the previously prepared parallel (blue, dark gray curve) and antiparallel (orange, light gray curve) spin-valve configuration assuming incoherent transport. As with increasing B_z, the spin polarization is decreased due to spin dephasing the spin-valve signal, i.e., the difference of the two curves, is quenched at high B_z. In both measurements, for the antiparallel and parallel states, the same intermediate resistance state R_{int} is reached at high B_z starting at the respective value $R_{AP,P}$ at $B_z = 0$. The data are shown for a spin-valve device with a negative MR effect ($R_{AP} < R_P$) as this behavior is usually observed in organic spin-valve devices.

using muon-spin rotation[20] or two-photon photoemission.[21] Also, the fabrication of a spin OLED (organic light-emitting diode[22]) indicates the presence of spin-polarized carriers in the respective OSC material. These three experiments do, however, not prove that this spin polarization is the cause of an electrical spin-valve effect. From inorganic semiconductor spintronics it is well known that the coexistence of spin polarization and magnetoresistance does not mean that the first is necessarily the cause of the second. All three methods mentioned above are only linked to the presence of the spin-polarized electrons but not to the electrical detection mechanism. The typical modulation of a spin-valve signal by spin precession, however, creates the necessary link between the two.

In fact, spin precession has been accepted as the only reliable proof because it is a very basic physical phenomenon. Spin-polarized conduction electrons in a perpendicular magnetic field do always precess unless the g factor in the material is zero. No further theory is needed to link experiment and conclusion. In other words, for a g-factor unequal to zero there is no way that conduction electrons do not precess in a suitable magnetic field. The typical B-field dependence is unique and does directly show up in the electrically detected spin-valve signature. This fact is also confirmed by the demonstration of spin precession of conduction electrons in OSC by paramagnetic resonance.[23] Thus, the investigation of the Hanle effect by magnetoresistance measurements (MR) in perpendicular magnetic fields B_z (also named perpendicular geometry hereafter) is an indispensable tool to interpret and understand the results of any spin-valve experiment.

If the spin precession does not show up in the electrical signature of a spin valve, there are only two possible reasons. Either the precession angle is too small to be detected or the electrical signal is not caused by the spin polarization. Too small a precession angle can be caused by a low g factor, by a very short transit time, or by hyperfine fields which are so large that the applied perpendicular field does not influence the spin polarization. Electron-spin resonance experiments have shown that the g factor in typical OSC materials is close to 2. The hyperfine field can be estimated and the perpendicular field magnitude can be chosen such that it greatly surpasses the hyperfine interaction (e.g., $B_z > 1$ mT).[8,24] So, the most critical point is an accurate estimate of the precession time.

The spin lifetime as such is expected to be longer in OSCs than in their inorganic counterparts. For the transit time, the following estimation shows that indeed only rather small B_z are needed for a sufficiently fast precession of the spins. Assuming $g = 2$ for any OSC, the precession time t_{prec} can be calculated from Eq. (1):

$$t_{\text{prec}} = \frac{2\pi m_e}{e B_z}. \tag{3}$$

This yields $t_{\text{prec}} \approx 3.6$ ns for $B_z = 10$ mT. t_{prec} has to be compared to the transit time which is needed for a spin to travel through the OSC layer with a thickness d_{OSC}. We make a rough estimation for t_{trans} as well:

$$t_{\text{trans}} = \frac{d_{\text{OSC}}}{v} = \frac{d_{\text{OSC}}}{\mu E} = \frac{d_{\text{OSC}}^2}{\mu U_{\text{bias}}}, \tag{4}$$

where v is the velocity of the spins and E the electric field.

Typical values for an OSV experiment are mobility $\mu = 1 \times 10^{-3}$ cm^2/Vs, $d_{\mathrm{OSC}} = 100$ nm, and applied bias voltage $U_{\mathrm{bias}} = 100$ mV. With these values we obtain $t_{\mathrm{trans}} = 1$ μs $\approx 300 \times t_{\mathrm{prec}}$ from Eq. (4). Thus, even for thin OSC layers the precession at small B_z is sufficiently fast compared to the transit time to cause a spin-dephasing effect. Assuming that half a precession period is more than enough to cause a change in the spin-valve signal, we see that even at much higher (unrealistic) mobilities, an effect should be visible, moreover as we do also observe a spin-valve effect at bias voltages as small as 1 mV.

Furthermore, we conclude from the comparison of t_{prec} and t_{trans} that the transport through the OSC layer is so slow that we do not expect to see any Hanle oscillations but only the Hanle effect caused by the spin dephasing (see Fig. 1). This conclusion is additionally sustained by the fact that the charge transport in amorphous or polycrystalline OSC layers is occurring by rather incoherent mechanisms such as variable range hopping[25] (VRH) or multiple trapping and release[26] (MTR).

In order to complete the preconditions for our experiment, one more point needs to be discussed. In lateral spin valves based on inorganic semiconductors, perpendicular fields are applied to an open transport channel.[12] In contrast, in a vertical OSV the field penetrates through the ferromagnetic electrodes. Nevertheless, magnetostatics show that no shielding takes place and the full field is present in the OSC. Only when the magnetic field is so large that it surpasses the shape anisotropy of the contacts and starts to magnetize the contacts out of the plane will an influence on the transport occur.[27] The latter, however, can easily be identified in the experiment by the changing spin-valve signal as in Ref. 28 and is furthermore completely excluded in the field range which is used in our experiments. All ferromagnets involved have a rather large volume magnetization[29–31] requiring a field of several 100 mT to create an out-of-plane magnetization of the respective layers.

As has already been indicated, an adequate measurement geometry has to be prepared for measurements in perpendicular fields, i.e., it is elementary to prepare the parallel (antiparallel) spin-valve state resulting in a device resistance of R_P (R_{AP}) at $B_{ip} = 0$ before the sweep of B_z is started. For a spin valve for which $R_P > R_{AP}$, as is typical for OSVs, increasing B_z results in a decrease of R_P and in an increase of R_{AP}. Both curves end up at the same intermediate resistance R_{int} at sufficiently large B_z as shown in Fig. 1.

II. EXPERIMENTAL DETAILS

We have fabricated two sets of vertical OSV structures with different OSC materials as spacer layer which also differ in terms of electrodes and fabrication process.

The first material under investigation is the n-type OSC N,N'-bis(n-heptafluorobutyl)-3,4:9,10-perylene tetracarboxylic diimide [PTCDI-C4F7, Fig. 3(a)] which is used due to its excellent properties with respect to charge carrier mobility and stability in ambient conditions.[32] PTCDI-C4F7 is a material well suited for spin-valve applications as already has been shown in our previous work.[9] The devices based on this material have a bottom contact made of 10-20-nm-thick $La_{0.7}Sr_{0.3}MnO_3$ (LSMO) layers, grown by pulsed plasma deposition[33] on strontium titanate (STO) or neodymium gallate (NGO) substrates, and a CoFe top contact. The active area of the PTCDI-C4F7-based OSVs is 150 μm $\times$ 500 μm. A series of devices with different OSC layer thicknesses d_{OSC} ranging from 100 to 600 nm was fabricated.

For device fabrication with PTCDI-C4F7 as OSC spacer, first Ti/Au metal stripes are deposited on the LSMO, using optical lithography, evaporation, and lift-off. These stripes serve as alignment marks and later as bond pads. A rectangular bottom contact is then patterned into the LSMO layer by optical lithography and dry etching, leaving the metal contact at one side of the rectangle. Subsequently, the sample is inserted into the UHV-deposition chamber where a bake-out procedure is performed at 450 °C for 1 h at an oxygen pressure of 10^{-5} mbar, in order to compensate underoxygenation which may occur during the processing. Subsequently, the PTCDI-C4F7 layer and the metal top electrode are deposited under different angles of incidence through a shadow mask with a rectangular opening. After removing the sample from the UHV chamber, Ti/Au stripes are deposited through a second shadow mask with striped windows. These metal stripes are later used as bond pads for the top contacts and also serve as an etch mask for the removal of the top electrode material between the stripes by dry etching. This approach provides clean, oxygen-free, and reproducible interfaces which are known to be crucial for working OSV devices.

Furthermore, we also fabricated devices with the well-known and extensively investigated material Tris(8-hydroxyquinoline)-aluminium(III) [AlQ_3, Fig. 2(a)], a low-mobility amorphous n-type OSC. The fabrication process for these devices is different from the one for the PTCDI-C4F7 devices and will be explained in detail elsewhere. The main differences compared to the PTCDI-C4F7 devices are the fabrication method of the LSMO electrode (thickness 20 nm, grown by pulsed laser deposition) and the patterning of the devices' active area (100 μm $\times$ 400 μm) by means of lithography instead of shadow masks and dry etching. The thickness of the OSC layer is ranging from 40 to 100 nm for the AlQ_3 devices.

The samples are characterized at various temperatures between 4.2 K and room temperature. Preliminary investigations of the observed MR effects were done in either a ^{4}He flow cryostate or a ^{4}He bath cryostate, both equipped with an external room-temperature electromagnet ($B_{\mathrm{max}} =$ 600 and 800 mT, respectively) at various temperatures. The experiments in the perpendicular geometry were conducted at 4.2 K in a ^{4}He bath cryostate with a three-dimensional (3D) vector magnet in which magnetic fields up to 400 mT can be applied in any direction in space.

III. RESULTS

A. Spin-valve effects

Figures 2 and 3 summarize typical data on the transport properties (magnetoresistance traces, I/V characteristics, and differential conductance dI/dU_{bias}) for both types of devices.

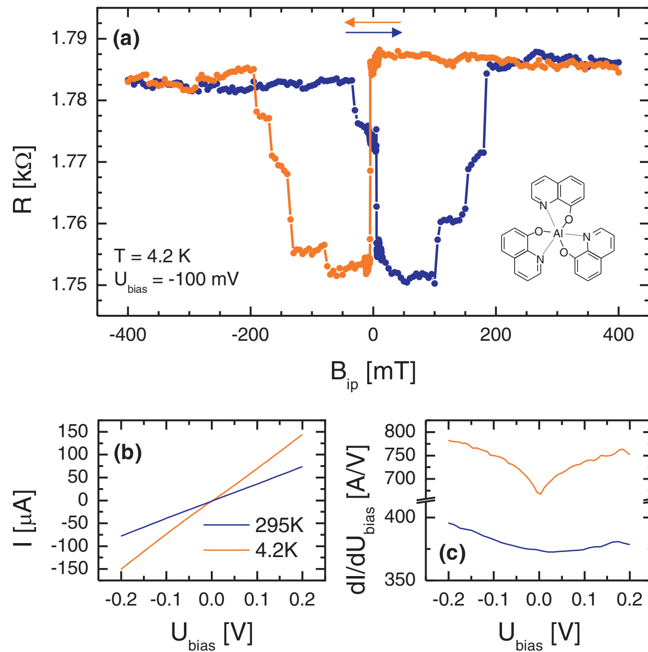

FIG. 2. (Color online) Typical performance of an OSV device based on AlQ_3. (a) Shows the MR trace as well as the molecular structure of AlQ_3. As indicated by the arrows, the sweep from positive saturation to negative saturation is represented by the orange/light gray curve, the opposite sweep direction by the blue/dark gray curve. The spin-valve behavior of this device ($d_{OSC} = 50$ nm) exhibits a total MR of $\sim -2.0\%$. Only sharp switching events between the parallel and antiparallel configurations and back are observed. The measurement is done at 4.2 K and $U_{bias} = -100$ mV. (b), (c) Show the transport properties of the present device represented by the I/V characteristics and the differential conductance dI/dU_{bias}, respectively, taken at room temperature (blue/dark gray line) and 4.2 K (orange/light gray line). dI/dU_{bias} is shown to underline the nonlinearity of the I/V curve. The weak temperature dependence of the devices resistance during cooling observed in these measurements is a clear indication of tunneling processes playing an important role for the charge transport.

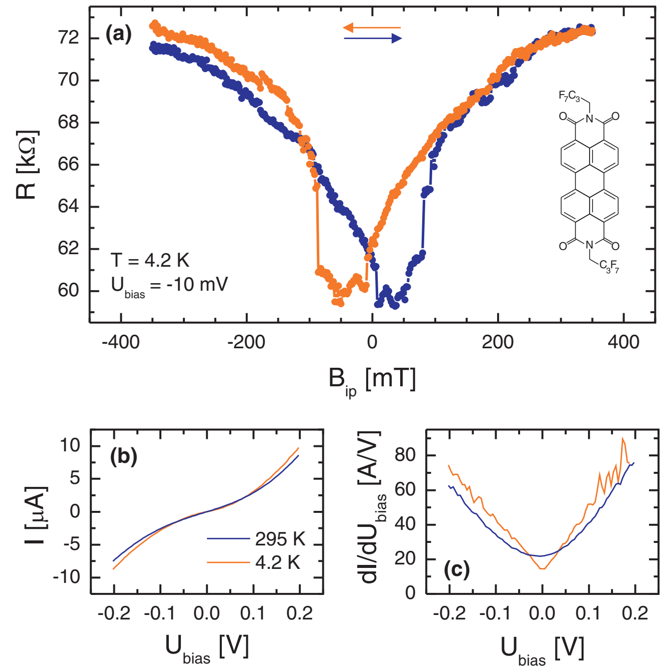

FIG. 3. (Color online) Typical performance of an OSV device based on PTCDI-C4F7. (a) Shows the spin-valve behavior as well as the molecular structure of PTCDI-C4F7. As indicated by the arrows, the sweep from positive saturation to negative saturation is represented by the orange/light gray curve, the opposite sweep direction by the blue/dark gray curve. In contrast to the behavior of AlQ_3-based device in Fig. 2(a), the MR trace of this device ($d_{OSC} = 150$ nm) exhibits spin-valve-like behavior with a total MR of $\sim -20\%$ taken at $U_{bias} = -10$ mV and 4.2 K and a relatively large nonlinear background. A constant increase of R with increasing B_{ip} is superimposed to the two distinct switching events between the parallel and antiparallel configurations and back (spin-valve signal). Again, (b) and (c) show the transport properties of the present device represented by the I/V characteristics and the differential conductance dI/dU_{bias}, respectively, taken at room temperature (blue/dark gray line) and 4.2 K (orange/light gray line). Obviously, the nonlinearity of the I/V curves is more pronounced for the PTCDI-C4F7 device compared to the AlQ_3 device [see Figs. 2(b) and 2(c)].

The magnetoresistance trace of an AlQ_3-based device (present device: $d_{OSC} = 50$ nm) is shown in Fig. 2(a). The actual spin-valve signal is very pronounced and almost no background effect is observed, only a small decrease of R with increasing B_{ip} can be discerned. The spin-valve effect itself is negative (low-resistance state appears for antiparallel magnetization of the electrodes R_{AP}). The change of the magnetization can be identified as sharp switching events in the MR trace. When B_{ip} is swept from high-positive to high-negative fields, the first switching event leading to the low-resistance state R_{AP} appears at small negative fields ($B_{ip} \approx -10$ mT). This switching can be ascribed to the magnetization reversal of the LSMO electrode. The Co electrode's magnetization is reversed at higher fields ($B_{ip} \approx -100$– -200 mT) via multiple steps finally resulting in the high-resistance (parallel magnetization) state R_P again. The MR effect has a magnitude of MR $= (R_{AP} - R_P)/R_{AP} \approx -2.0\,\%$ at 4.2 K and $U_{bias} = -100$ mV and is symmetric with respect to $B_{ip} = 0$ mT, i.e., for the opposite sweep direction the same behavior is observed in the positive-field range.

The magnetoresistance trace of a PTCDI-C4F7 based device (present device: $d_{OSC} = 150$ nm) has a different shape [Fig. 3(a)]. The observed effect with a total MR ratio of $\approx -20\,\%$ at 4.2 K and $U_{bias} = -10$ mV again is symmetric with respect to $B_{ip} = 0$ mT but has two distinct components. On one hand, the MR trace comprises a nonlinear background effect, increasing resistance with increasing B_{ip}, which is well known for various OSV devices based on other OSCs reported in the literature[4,34–36] and can be explained by the magnetic electrodes being saturated at higher magnetic fields. The organic magnetoresistance effect[37] (OMAR) is likely to be excluded as the origin for the background signal in our devices as has been shown in previous studies.[9] On the other hand, we see the actual negative spin-valve effect which is less pronounced compared to the AlQ_3-based OSV due to the superimposed background signal. Comparable to the AlQ_3 device, the first switching event from high (R_P) to low resistance (R_{AP}) occurs at small B_{ip}. When B_{ip} is further increased, the magnetization reversal of the second electrode

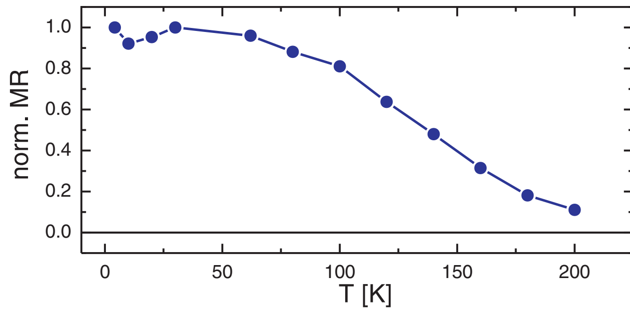

FIG. 4. (Color online) Temperature dependence of the spin-valve signal of a PTCDI-C4F7 OSV device ($d_{\mathrm{OSC}} = 150$ nm). The data are normalized to the maximum MR value recorded at $T = 4.2$ K ($\sim -12.7\%$ for this device). The observed behavior, decreasing MR ratio with increasing temperature, is similar to other OSV devices in the literature. At $T = 200$ K the effect has diminished to 10% of its maximum value.

(CoFe) occurs at $B_{ip} \approx -100$ mT, which is lower than the magnetic field required to reverse the magnetization of the Co electrode in the AlQ_3 devices.

The spin-valve signals presented in Figs. 2(a) and 3(a), which can be considered typical for our OSV devices with the respective OSC, have been studied extensively with respect to various parameters. For instance, we obtained a typical dependence of the observed MR effect on the temperature and d_{OSC} of the layer under investigation. Figure 4 shows the temperature dependence of the MR for a PTCDI-C4F7-based device. With increasing temperature, the MR is decreased. It vanishes nearly completely at $T \approx 200$ K. For the AlQ_3-based devices, similar behavior is observed. The dependence of MR on OSC layer thickness shows a clear tendency of reduced MR for increasing layer thickness. The variation of the respective MR, however, even for devices with the same layer thickness does not allow us to fit the data or even to extract a kind of spin-flip length. We also observe a strong decrease of the MR ratio with increasing bias voltage in the <1 V regime.

Moreover, we have studied the I/V characteristics and their temperature dependence. For the AlQ_3 device, the I/V characteristics [Fig. 2(b)] look nearly linear for high and low temperature and the resistance is decreasing with decreasing temperature. The latter is most likely due to a lowered resistance of the LSMO at reduced temperatures. For the PTCDI-C4F7 device, we do not observe any sizable change in the resistance when cooling the sample from room temperature to 4.2 K [Fig. 3(b)]. The fact that this observation holds for PTCDI-C4F7 layers as thick as 600 nm is a clear indication of pinholes or at least areas of reduced thickness. Transport for an undisturbed PTCDI-C4F7 layer of similar thickness would normally result in immeasurably small current values at 4.2 K. The I/V characteristics obviously are nonlinear for both temperatures.

dI/dU_{bias} plots [Figs. 2(c) and 3(c)] for both OSC materials reveal nonlinearity of the I/V characteristics also for AlQ_3 and the data strongly indicate that at low T and low U_{bias}, the charge transport is dominated by tunneling processes. As already mentioned above, more decisive information can be gained by measurements in perpendicular magnetic fields which are conducted for several devices of both types showing a distinct spin-valve behavior comparable to the traces in Figs. 2(a) and 3(a).

B. Experiments in the perpendicular geometry: ALQ_3 OSVS

In order to detect the presence of Hanle precession, it is necessary to apply the perpendicular magnetic field to the in-plane antiparallel magnetized and the in-plane parallel magnetized states of the spin valve, respectively. The fact that OSV often exhibit a negative spin-valve effect shows that sign and magnitude of the spin accumulation in the OSC can not be related to the magnetization states in a straightforward manner. As a consequence, it is not possible to predict whether the influence of spin precession on the two individual resistance states is equally strong. It is, however, obvious that the difference in resistance between the two states should diminish when Hanle precession is present. Thus, it is important to investigate both remanent states in detail. In a recent publication,[28] data have already been presented for magnetic field sweeps perpendicular to the sample plane, however, starting the sweep from perpendicular saturation. In our case, the use of a 3D vector magnet allows us to prepare both remanent states individually by running a field sweep from parallel saturation to the desired state and then reducing

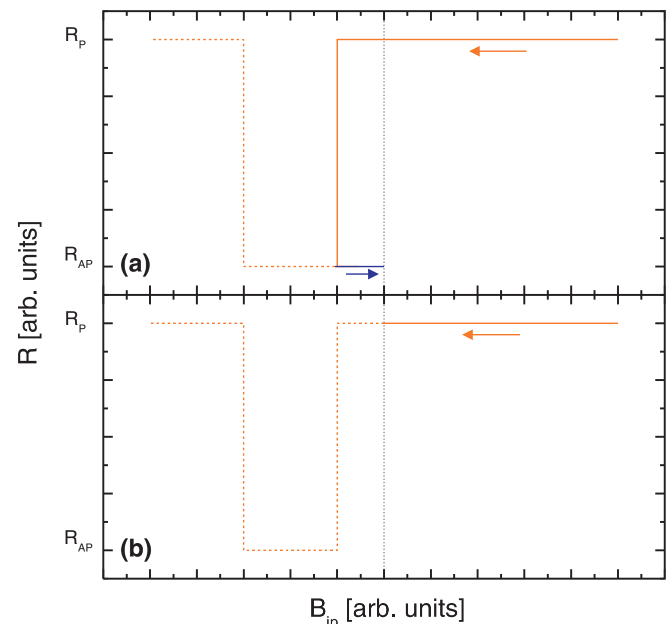

FIG. 5. (Color online) Schematic presentation of the B_{ip} sweeps required for the preparation of the antiparallel (a) and parallel (b) magnetization states of a spin valve's electrodes (starting at positive saturation). The solid lines show the sweeps necessary for preparation, while the dashed lines represent a complete trace of the negative spin-valve signal ($R_{AP} < R_P$). The antiparallel state (a) is initialized by sweeping a minor loop of B_{ip}: B_{ip} is decreased from positive saturation to small negative values until the first switching event occurs (orange/light gray line). Subsequently, B_{ip} is returned to 0 (blue/dark gray line) leaving the spin valve in the remanent antiparallel state (R_{AP}). The parallel configuration (b) is prepared similarly by sweeping B_{ip} from saturation field to 0. As no reversal of the electrodes' magnetization occurs at positive B_{ip} for this sweep direction, the devices resistance remains in the remanent R_P state.

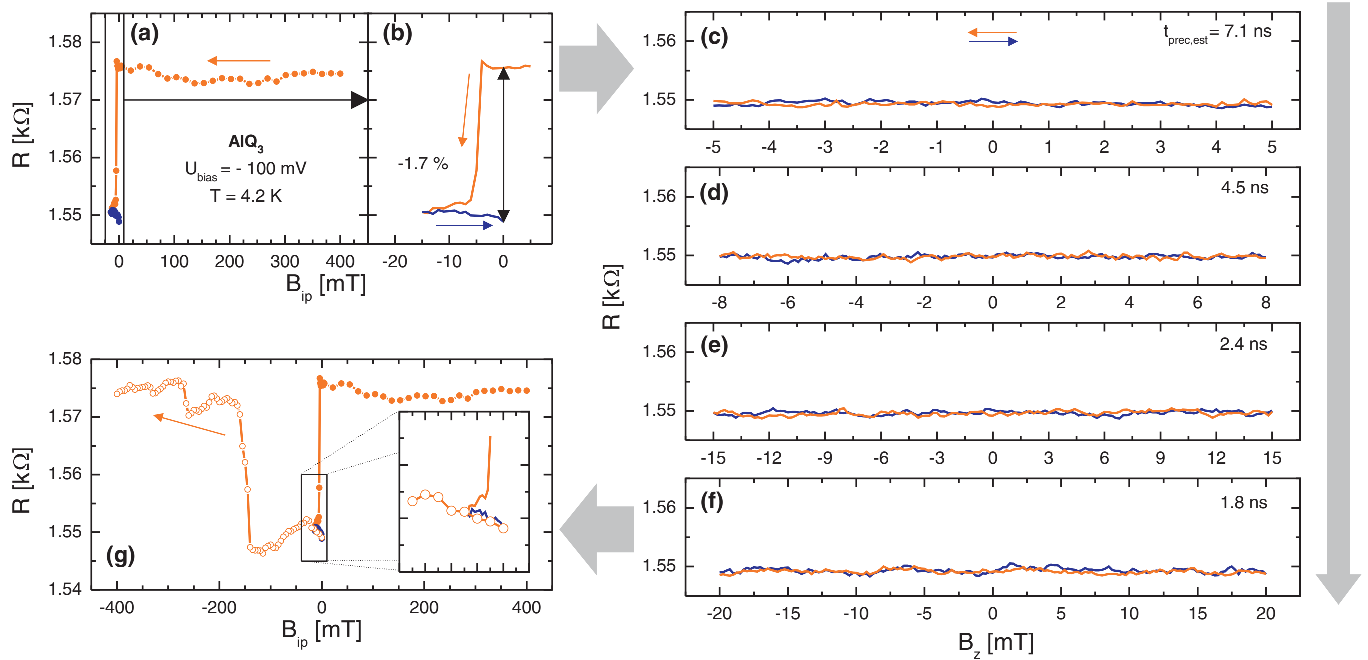

FIG. 6. (Color online) Sequence of measurements investigating the remanent antiparallel state of a AlQ_3 OSV in a perpendicular magnetic field, recorded at 4.2 K and $U_{\text{bias}} = -100$ mV. Gray arrows are a guide to the eyes and indicate the order of experiments. The initial minor loop shown in (a) and (b) necessary for the preparation of the antiparallel state exhibits a MR ratio of $\sim -1.7\%$ at $B_{ip} = 0$ mT. (c)–(f) Contain the data of the experiments in the perpendicular geometry. Please note that the scale for R is the same in all plots. The maximum absolute B_z and the corresponding minimum precession time t_{prec}, calculated using Eq. (3), is increased/decreased in every single measurement. We observe a constant device resistance in all measurements (c)–(f) of the series in which the minimum t_{prec} was varied from ~7.1 to ~1.8 ns. The statistical variations of R in the range of $\sim\pm0.25\%$ are much smaller than the total magnetoresistance effect. Having finished the measurements in the perpendicular geometry, the initial minor-loop measurement is completed with a sweep of B_{ip} from 0 mT to large negative values [line with open circles in (g)]. As this scan clearly reproduces the MR scan in Fig. 2(a), we can be sure that the magnetization configuration of the electrodes and by this the spin-valve state was not disturbed by applying B_z.

the in-plane field to zero. Subsequently, the perpendicular field is applied and swept over the desired range. After the perpendicular field sweep is finished, the in-plane MR loop is completed in order to verify that the magnetization state of the electrodes is unchanged (the corresponding field sweeps for the preparation of the spin valves' antiparallel and parallel states are shown in Fig. 5).

Figure 6 summarizes a complete sequence of measurements in the perpendicular geometry for the antiparallel configuration in a AlQ_3-based device. All measurements are performed at $U_{\text{bias}} = -100$ mV and $T = 4.2$ K. The antiparallel state is prepared by sweeping B_{ip} on a minor loop [Figs. 6(a) and 6(b)]: Starting at high positive fields, B_{ip} is swept beyond 0 mT (orange/light gray curve) until the magnetization of the LSMO electrode is reversed, yielding the low-resistance state. Subsequently, B_{ip} is set to 0 mT (blue/dark gray curve). As can be seen in Fig. 6(b), the device remains in the low-resistance state when B_{ip} is turned off. Hence, a stable remanent antiparallel configuration of the electrodes' magnetization with $R_P \approx 1.575$ kΩ and $R_{AP} \approx 1.55$ kΩ corresponding to minor-loop MR ratio of $\sim -1.7\,\%$ is prepared.

The measurements with the magnetic field applied perpendicular to the sample plane involve sweeps of B_z from 0 mT to higher fields (up to ±20 mT) and back while the in-plane field remains at $B_{ip} = 0$ mT. Figures 6(c)–6(f) show the results of these experiments. The data use the same scale as the full magnetoresistance sweep. In each measurement, the maximum absolute value of B_z and by this ω_L is increased while the spins' precession time t_{prec} is decreased. The values of t_{prec} in Figs. 6(c)–6(f) are the minimum values calculated from Eq. (3) for the respective maximum value of B_z and are ranging from $t_{\text{prec}} \approx 7.1$ to 1.8 ns. In all measurements we obtain, independently of the sweep direction of B_z and its maximum value, a constant device resistance with only statistical variations of $\sim\pm0.25\%$ around $R(0\text{ mT})$.

After returning B_z to zero, the minor loop we have used to prepare the in-plane antiparallel state is completed to a major loop in order to realize a full magnetoresistance scan. This measurement is done in order to ensure that the electrodes' magnetization has not been modified by the application of B_z and therefore the antiparallel state of the OSV device was not disturbed. The line with the open circles in Fig. 6(g) which shows the data for this measurement clearly reproduces the MR scan for this device recorded without any interruption [Fig. 2(a)]. Furthermore, this result also allows us to conclude that the small variations in R observed in the single measurements in Figs. 6(c)–6(g) are not caused by any influence of the applied B_z on the electrodes' magnetization. The initialization sequence for the parallel configuration is similar to the minor-loop scan in which the antiparallel state is prepared. For the preparation of the parallel state, B_{ip} is

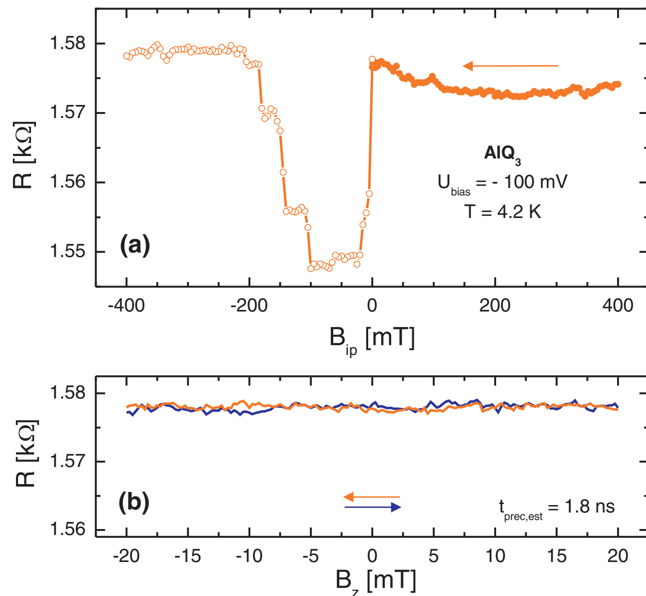

FIG. 7. (Color online) Results of measurements in the perpendicular geometry for the remanent parallel state of a AlQ_3 OSV recorded at 4.2 K and $U_{\rm bias} = -100$ mV. A sweep of B_{ip} from high positive fields to $B_{ip} = 0$ mT is first performed in order to set the device's state of parallel electrodes' magnetization at $B_{ip} = 0$ mT [closed circles in (a)]. (b) Shows data of a measurement in a perpendicular magnetic field for maximum $B_z = 20$ mT corresponding to a minimum $t_{\rm prec} \approx 1.8$ ns. As for antiparallel configuration, the device's resistance is constant apart from statistical variations in the range of $\sim\pm 0.25\%$. Again, the experiment is completed by the termination of the initial MR sweep [open circles in (a)] reproducing the MR trace of the device [Fig. 2(a)].

swept from saturation in the positive-field range to $B_{ip} = 0$ mT ending at $R_P \approx 1.575$ kΩ [Fig. 7(a), closed circles].

Figure 7(b) shows data of one measurement in the perpendicular geometry with a maximum B_z of ± 5 mT, which is done for the parallel state. This corresponds to a minimum precession time of $t_{\rm prec} \approx 7.1$ ns. Obviously, we do not observe any sizable change of the OSV's resistance for this configuration as well. After the sweep of B_z the MR loop is completed similarly as for the antiparallel state. The data of this measurement are shown in Fig. 7(a) (open circles) again reproducing the previously recorded full MR trace.

With a minimum precession time of $t_{\rm prec} \approx 1.8$ ns, we are clearly in a limit where the magnetoresistance should be quenched completely by the Hanle effect. The fact that the observed variations in perpendicular fields are statistical and much smaller than the total magnetoresistance clearly indicates that no spin-polarized charge transport is responsible for the observed magnetoresistance in the present devices.

C. Experiments in the perpendicular geometry: PTCDI-C4F7 OSVS

For the PTCDI-C4F7-based device, similar measurements in perpendicular geometry are performed. Figure 8(a) shows the preparation of the antiparallel remanent state by reversing the magnetization of the LSMO layer in a minor loop. As can be seen in the enlarged presentation in Fig. 8(b), the minor-loop MR ratio in this device is $\sim -4.7\,\%$ when the in-plane field is set back to $B_{ip} = 0$ mT. The corresponding resistance values are $R_P \approx 62.5$ kΩ for the parallel remanent state and $R_{AP} \approx 59.7$ kΩ for the antiparallel remanent state.

The measurements in the perpendicular geometry are shown in Figs. 8(c)–8(g). The maximum absolute values of B_z correspond to precession times $t_{\rm prec} \approx 11.9$–$1.8$ ns. The data in Figs. 8(c)–8(g) show that for any value of B_z the device resistance varies by less than $\sim\pm 1\,\%$. The sweep completing the initial minor loop is shown in Fig. 8(h) (line with open circles).

Figure 9 summarizes the respective experiments in the parallel configuration of the PTCDI-C4F7 device. After sweeping B_{ip} from large positive values to $B_{ip} = 0$ mT [Fig. 9(a), line with closed circles] measurements with the magnetic field applied perpendicular to the sample plane are performed. Although the device's resistance has slightly drifted in the time between the measurements for the antiparallel and the parallel states, this change does not substantially influence the device's spin-valve performance as is ensured by a full MR sweep [Fig. 9(a), blue/dark gray line in the background of the panel). The maximum B_z for the data in Fig. 9(b) is ± 5 mT corresponding to a precession time of $t_{\rm prec} \approx 7.1$ ns. These data show that we do not observe any sizable change of the device's resistance for the parallel configuration as well. Again, the measurement is completed by the final sweep of B_{ip} to negative values [Fig. 9(a), line with open circles]. The data of this measurement continue the initial B_{ip} sweep and reproduce the typical MR trace of the device [Fig. 3(a), blue/dark gray line in Fig. 9(a), respectively].

Although for the PTCDI-C4F7-based device the magnetoresistance trace is less pronounced than for the AlQ_3-based one, the variation of the resistance in the parallel and the antiparallel states, respectively, again shows that no Hanle precession can be observed, and thus also in this device spin-polarized charge transport is not the cause of the magnetoresistance which can be observed in our devices.

D. Discussion

Our results show that in none of the presented experiments do we observe any Hanle precession although the devices exhibit a pronounced spin-valve effect. As mentioned in our initial discussion, there are two possible explanations for the absence of spin precession in experimental data: either the observed spin-valve signal is not caused by spin polarization or the precession angle is to small to allow for an electrical detection of the precession. The latter would mean that the transit time is too low to allow for at least half a precession period. Based on the estimations made above, we believe this scenario is not an option. As also discussed by Riminucci *et al.*,[28] the mobilities would need to be unreasonably high for an amorphous or even a crystalline OSC in this case.

Therefore, we must conclude from our experiments that the absence of Hanle precession in our OSC devices excludes electrical spin detection as the main mechanism for the magnetoresistance. Consequently, there must be other effects at work. Stray fields which can cause a magnetoresistance signal via OMAR (Ref. 19) can be excluded in our experiments because of the low-bias voltages that we use. OMAR typically

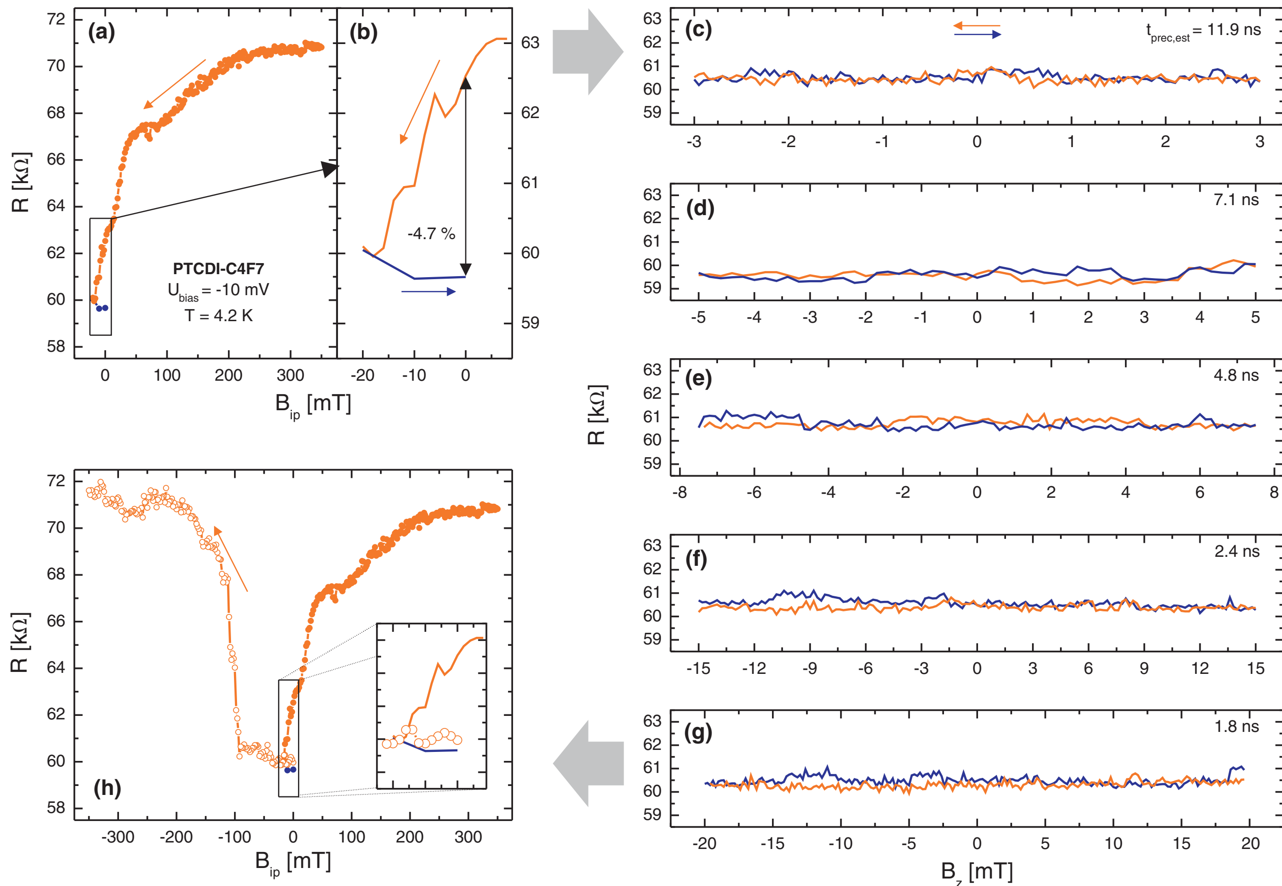

FIG. 8. (Color online) Complete measurement sequence of an experiment in the perpendicular geometry for the remanent antiparallel state of a PTCDI-C4F7 device recorded at 4.2 K and $U_{\rm bias} = -10$ mV. Gray arrows are a guide to the eyes and indicate the order of experiments. (a), (b) Show the minor-loop sweep for the preparation of the antiparallel state with a minor-loop MR ratio of -4.7% at $B_{ip} = 0$ mT. (c)–(g) Comprise the results of the measurements in perpendicular magnetic fields; again, the scale for R in (c)–(g) is the same as in (a) and (h). Measurements at $B_{ip} = 0$ mT with different maximum B_z corresponding to minimum spin precession times $t_{\rm prec}$ ranging from $\sim$11.9 to $\sim$1.8 ns were performed. $t_{\rm prec}$ is calculated using Eq. (3). As can be seen in (c)–(g), we only observe statistical variations of the resistance in the range of $\sim \pm 1\%$. The sequence is finished by completing the initial minor-loop measurement with a sweep of B_{ip} from 0 mT to high negative values [line with open circles in (h)]. This measurement shows that the magnetization state of the electrodes was not disturbed by applying B_z as can be seen from a comparison of the data in (h) with the MR scan in Fig. 3(a).

occurs at elevated voltages, while our magnetoresistance traces are still present at a few mV of bias.

More likely is the presence of TMR which can be caused by direct tunneling from the LSMO layer to the ferromagnetic counterelectrode at pinholes [Figs. 10(a) and 10(c), left-hand sides]. In order to truly appreciate the numbers involved, it is helpful to do a back-of-the-envelope calculation. A good estimate for the resistance of a pinhole can be extracted from Barraud *et al.*[38] who artificially create pinholes with a typical resistance of 100 MΩ per pinhole. They observe tunneling through these pinholes with a rather large TMR of up to 300%. In a simple picture of tunneling transport through pinholes (with TMR) and transport in parallel through the OSC (without magnetoresistance), the total magnetoresistance is reduced by the parallel current path. If the parallel resistance of the OSC is roughly a tenth of the parallel resistance of all pinholes, the magnetoresistance is also reduced approximately to one tenth of the original value. Identifying these pinholes for example by transmission electron microscopy (TEM) proves highly unlikely as the following estimate shows. We have a device with a resistance of $\sim$1 kΩ and a magnetoresistance of the order of magnitude of 10%. In our picture, this can be explained by a magnetization-independent resistance of $\sim$1 kΩ and pinholes with magnetoresistance that account for a total resistance of $\sim$10 kΩ. For a device area of 200 μm $\times$ 200 μm, which is comparable to our devices' active area, this equals an average of one pinhole on an area of 2 μm $\times$ 2 μm. Obviously, looking for such a distribution of pinholes by high-resolution TEM is likely to fail. Although AFM studies of our OSC films confirm indeed a smooth-layer surface before metallization, we know from former experiments that the evaporation of metal on top of formerly flat OSC layers can even lead to complete short circuits. It should be noted that for a certain thickness range of the OSC, the number of pinholes statistically depends on the thickness.[39] For thicker layers, the number of pinholes and thus the MR contribution is reduced, which can erroneously be interpreted as the effect of a finite spin-flip length.

The TMR option is also supported by the observed bias and temperature dependence. The physics of transport in OSCs

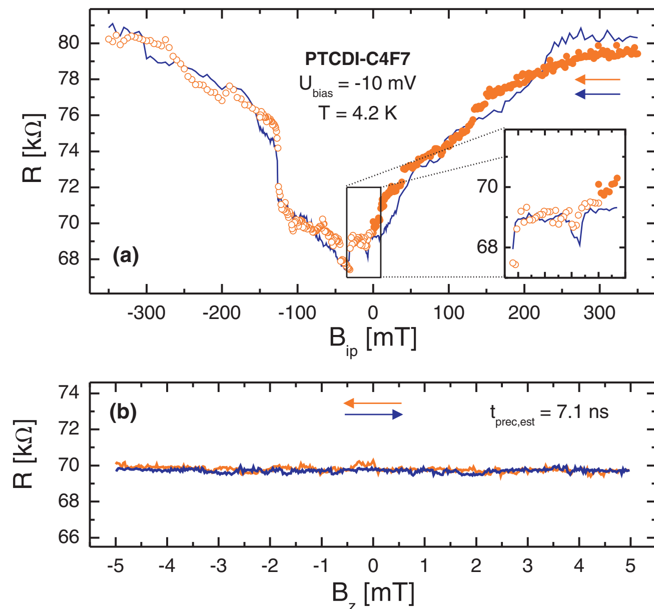

FIG. 9. (Color online) Experiments with the magnetic field applied perpendicular to the sample plane for the parallel state of a PTCDI-C4F7 device, recorded at 4.2 K and $U_{\text{bias}} = -10$ mV. The blue (dark gray) line in the background of panel (a) represents the formerly recorded full MR sweep. The state of parallel magnetization of the electrodes is prepared by sweeping B_{ip} from high positive fields to $B_{ip} = 0$ mT [full circles in (a)]. Subsequently, the measurements in perpendicular geometry are performed (b). The resistance obtained in a measurement with maximum $B_z = 5$ mT corresponding to a minimum $t_{\text{prec}} \approx 7.1$ ns is constant and only variations ($\sim\pm1\%$) much smaller than the actual spin-valve effect are observed. The experiment is finished by the completion of the initial MR sweep [open circles in (a)] verifying that the magnetization state of the electrodes was not modified by the applied B_z. The measured MR trace clearly reproduces the formerly recorded curve [blue/dark gray line in (a)].

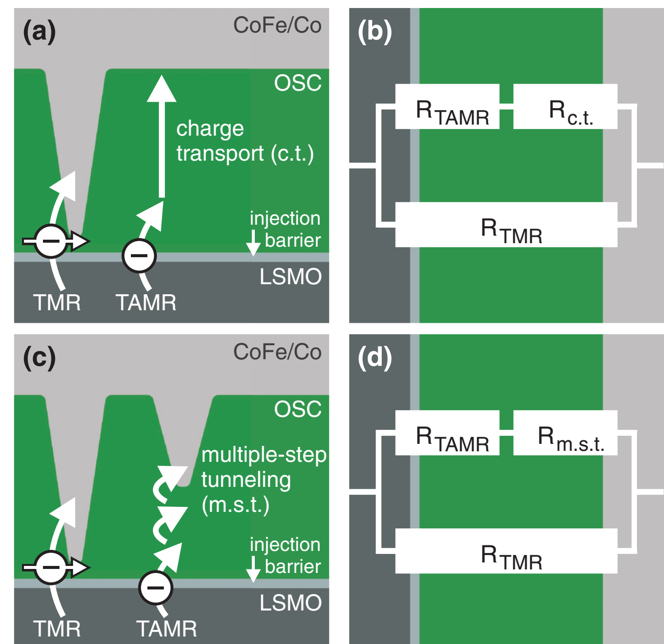

FIG. 10. (Color online) Schematic representation of possible charge-transfer mechanisms present in our devices [(a) and (c)] and of the resulting equivalent circuit diagrams [(b) and (d)]. In all cases, we have an injection barrier which is typical for contacts to OSCs and which is the prerequisite for the occurrence of TAMR. After charge injection via the barrier, various transport mechanisms can take over. In a layer with uniform thickness, subsequent transport will be dominated by VRH and MTR. If the layer thickness is strongly reduced in many areas, multiple-step tunneling (Ref. 8) can be predominant. In both cases, however, pinholes can provide a parallel current path prone to show TMR. It is important to keep in mind that TAMR does not require direct tunneling from one electrode to the other but only charge injection from a suitable material/electrode, LSMO in our case, into a nonmagnetic material, the OSC layer. Hence, in this approach the devices' resistance can be represented by a parallel connection of two resistors as shown in (b) and (d): R_{TMR} (direct tunneling) and $R_{\text{TAMR}} + R_{c.t./m.s.t.}$ (tunneling into the OSC layer and subsequent charge transport).

usually causes a strong temperature dependence of the resistance. Undisturbed layers of PTCDI-C4F7 typically show an increase in resistance by more than three orders of magnitude when cooled down from room temperature to 4.2 K. Those of our devices which show a magnetoresistance, however, either show no increase or even a decrease (because of the decreasing resistance of the LSMO) or only a small increase by less than a factor of 10. This behavior is well known for tunnel junctions. In this respect, we also would like to refer to Lin *et al.*[40] who were the first to demonstrate this link between spin-valve operation and low-temperature dependence of the device resistance and also the first to use these results to question the idea of spin-polarized transport as a basis for spin-valve operation. This hypothesis is further supported by our observation that for AlQ_3-based devices, the resistance decreases with decreasing temperature. If tunneling is the predominant mechanism, the increased metallicity of LSMO at low temperature goes along with an increasing density of occupied states which can contribute to the tunneling and thus reduce the tunneling resistance. In addition, the dI/dU_{bias} characteristics of the OSVs under consideration can be fitted using a parabola at low U_{bias}, which is standard for tunnel junctions. We have thus a number of indications that TMR can be at least a major contribution to the magnetoresistance.

Furthermore, a detailed investigation of the MR effect regarding its dependence on the orientation of B_{ip} with respect to the crystalline axes of the LSMO electrode unambiguously reveals that also TAMR (Refs. 9 and 41) is contributing to the spin-valve signal. TAMR occurs when charge carriers tunnel from a ferromagnetic material with crystalline anisotropy in the presence of spin-orbit coupling. For biaxial anisotropy plus a symmetry breaking,[41] the effect can mimic typical spin-valve behavior. LSMO fulfills these requirements and indeed we can clearly demonstrate the presence of TAMR. Figure 11 shows so-called φ-scans of our devices. In these scans, a large in-plane magnetic field is applied in order to saturate both electrodes in a parallel configuration. The direction of the magnetic field is then rotated by 360° while constantly monitoring the device resistance. In a pure TMR or GMR device, this measurement must show a constant resistance resulting in a perfect circle in an angle-dependent plot. Our

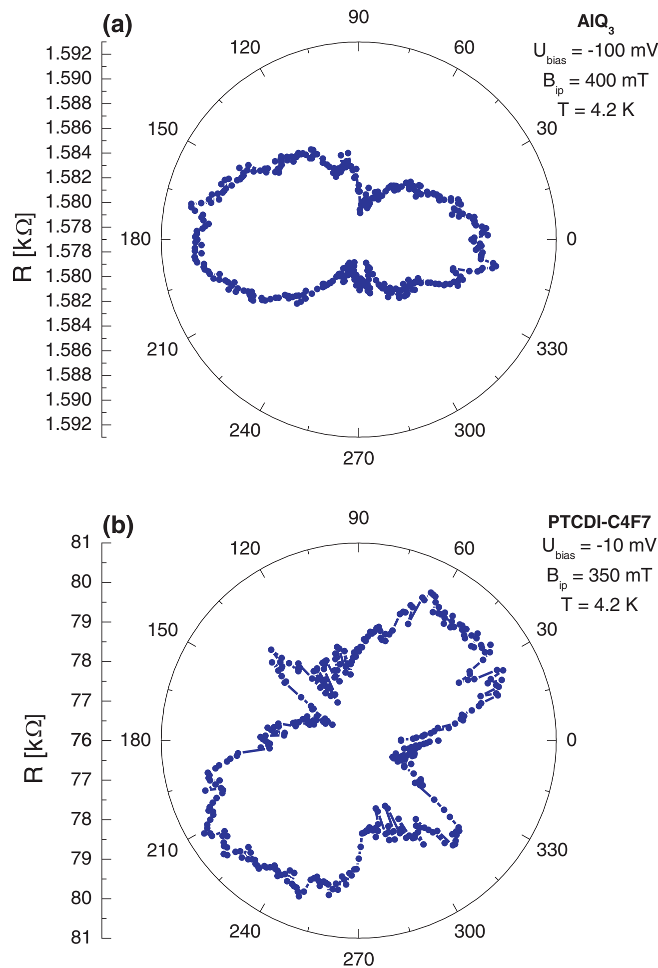

FIG. 11. (Color online) Results of φ-scan measurements for both types of devices. (a) Shows data for an AlQ_3 device taken at 4.2 K, $U_{bias} = -100$ mV, and $B_{ip} = 400$ mT. The data for the PTCDI-C4F7 device in (b) are recorded at 4.2 K, $U_{bias} = -10$ mV, and $B_{ip} = 350$ mT. As discussed in the text, φ-scan measurements give unambiguous information whether TAMR is present in a device or not. Therefore, as we obtain an anisotropic resistance at high B_{ip}, i.e., with the ferromagnetic electrodes in saturation, a TAMR contribution to the observed spin-valve signals must be taken into account.

measurements, however, show a strong angle dependence demonstrating the presence of TAMR. In contrast to the TMR contribution, TAMR does not involve spin-dependent tunneling or tunneling between both electrodes. The tunnel process of charge injection from LSMO into the OSC is the only necessary ingredient [Figs. 10(a) and 10(c), right-hand side]. The temperature dependence of the resistance and the I/V characteristics that we expect for TMR and TAMR are necessarily identical.

Thus, the most likely scenario for our devices is charge transport through the OSC which may involve spin injection but definitely does not involve electrical detection. The mechanisms dominating this charge transport can vary depending on the morphology of the OSC layer and the top electrode, respectively. The right-hand sides of Figs. 10(a) and 10(c) show two model cases. At the injection barrier carriers can tunnel in to the OSC likely to create a contribution of TAMR. Depending on the morphology the charge injection can be followed by normal charge transport through the OSC via VRH/MTR or when a nonuniform thickness distribution is present by multistep tunneling.[8] Of course, one also can imagine an intermixing of both cases. In parallel to this conduction path, we may always have TMR caused by pinholes extending almost completely through the OSC layer.

Finally, it should be mentioned that although the reproducibility of total device resistance is not ideal, the majority of our devices show spin-valve behavior. Further to the studies presented here we have performed measurements in perpendicular fields for a large number of the working spin valves. None of these measurements showed the smallest sign of any influence of the perpendicular field on the spin-valve effect.

IV. CONCLUSION

We have shown the results of magnetoresistance measurements with the magnetic field applied perpendicular to the sample plane after preparing in-plane parallel or antiparallel magnetization states. The devices under investigation differ in OSC material but also in the shape of the observed spin-valve signal. In none of our measurements do we observe any Hanle effect in the perpendicular geometry. Although the observations tell nothing about the possible injection of spin-polarized carriers into the organic material, we must, as a consequence, exclude any spin-polarized transport through the OSC layer with subsequent electrical spin detection as origin of the observed spin-valve effects in the present devices. It is thus likely that TMR by tunneling through pinholes superimposed by TAMR occurring at charge injection into the OSC is the cause of the spin-valve behavior of our devices.

We would like to emphasize that these results apply to our spin valves and that we can not determine whether electrical spin detection has been demonstrated by others or not. Indeed, there are, for example, experiments which by the use of different hydrogen isotopes in an OSC material show different magnitudes of the spin-valve signal.[7] This is a strong indication that indeed true spin detection is present. Nevertheless, this experiment still relies on the assumption that hyperfine interaction is the major spin-flip mechanism and that no other effect of the nuclear spin (for example, on spin tunneling) can exist. Even there, Hanle precession could provide an even more direct and irrefutable proof.

In conclusion, we think that our studies show that careful investigations of any observed spin-valve effect are mandatory to draw any conclusion concerning the mechanisms causing MR effects. Measurements in perpendicular magnetic fields and the investigation of the Hanle effect are a very helpful tool in this context as they allow for decisive statements with respect to electrical spin detection and spin-polarized transport through OSC layers.

ACKNOWLEDGMENTS

We thank the EU for funding the research in the projects OFSPIN (Project No. NMP-CT-2006-033370) and HINTS (Project No. NMP3-SL-2011-263104). We acknowledge P. Grazioso and A. Dediu from CNR Bologna for provision of the LSMO layer for the PTCDI-C4F7-based OSV device.

*Corresponding author: georg.schmidt@physik.uni-halle.de

[1]V. Dediu, M. Murgia, F. Matacotta, C. Taliani, and S. Barbanera, Solid State Commun. **122**, 181 (2002).
[2]Z. Xiong, D. Wu, Z. Vardeny, and J. Shi, Nature (London) **427**, 821 (2004).
[3]S. Majumdar, H. S. Majumdar, R. Laiho, and R. Österbacka, J. Alloys Compd. **423**, 169 (2006).
[4]W. Xu, G. Szulczewski, P. LeClair, I. Navarrete, R. Schad, G. Miao, H. Guo, and A. Gupta, Appl. Phys. Lett. **90**, 072506 (2007).
[5]F. Wang, Z. Xiong, D. Wu, J. Shi, and Z. Vardeny, Synth. Met. **155**, 172 (2005).
[6]T. S. Santos, J. S. Lee, P. Migdal, I. C. Lekshmi, B. Satpati, and J. S. Moodera, Phys. Rev. Lett. **98**, 016601 (2007).
[7]T. Nguyen, G. Hukic-Markosian, F. Wang, L. Wojcik, X. Li, E. Ehrenfreund, and Z. Vardeny, Nat. Mater. **9**, 345 (2010).
[8]J. J. H. M. Schoonus, P. G. E. Lumens, W. Wagemans, J. T. Kohlhepp, P. A. Bobbert, H. J. M. Swagten, and B. Koopmans, Phys. Rev. Lett. **103**, 146601 (2009).
[9]M. Grünewald, M. Wahler, F. Schumann, M. Michelfeit, C. Gould, R. Schmidt, F. Würthner, G. Schmidt, and L. W. Molenkamp, Phys. Rev. B **84**, 125208 (2011).
[10]M. A. Baldo and S. R. Forrest, Phys. Rev. B **64**, 085201 (2001).
[11]F. Monzon and M. Roukes, J. Magn. Magn. Mater. **198–99**, 632 (1999).
[12]X. Lou, C. Adelmann, S. A. Crooker, E. S. Garlid, J. Zhang, K. S. M. Reddy, S. D. Flexner, C. J. Palmstrom, and P. A. Crowell, Nat. Phys. **3**, 197 (2007).
[13]B. Huang, D. J. Monsma, and I. Appelbaum, Phys. Rev. Lett. **99**, 177209 (2007).
[14]M. Johnson and R. H. Silsbee, Phys. Rev. Lett. **55**, 1790 (1985).
[15]M. Johnson and R. H. Silsbee, Phys. Rev. B **37**, 5326 (1988).
[16]N. Tombros, C. Jozsa, M. Popinciuc, H. T. Jonkman, and B. J. van Wees, Nature (London) **448**, 571 (2007).
[17]Y. Ohno, D. Young, B. Beschoten, F. Matsukura, H. Ohno, and D. Awschalom, Nature (London) **402**, 790 (1999).
[18]R. Fiederling, M. Keim, G. Reuscher, W. Ossau, G. Schmidt, A. Waag, and L. Molenkamp, Nature (London) **402**, 787 (1999).
[19]F. Wang, F. Macià, M. Wohlgenannt, A. D. Kent, and M. E. Flatté, Phys. Rev. X **2**, 021013 (2012).
[20]A. J. Drew, J. Hoppler, L. Schulz, F. L. Pratt, P. Desai, P. Shakya, T. Kreouzis, W. P. Gillin, A. Suter, N. A. Morley, V. K. Malik, A. Dubroka, K. W. Kim, H. Bouyanfif, F. Bourqui, C. Bernhard, R. Scheuermann, G. J. Nieuwenhuys, T. Prokscha, and E. Morenzoni, Nat. Mater. **8**, 109 (2009).
[21]M. Cinchetti, K. Heimer, J.-P. Wuestenberg, O. Andreyev, M. Bauer, S. Lach, C. Ziegler, Y. Gao, and M. Aeschlimann, Nat. Mater. **8**, 115 (2009).
[22]T. D. Nguyen, E. Ehrenfreund, and Z. V. Vardeny, Science **337**, 204 (2012).
[23]W. J. Baker, K. Ambal, D. P. Waters, R. Baarda, H. Morishita, K. van Schooten, D. R. McCamey, J. M. Lupton, and C. Boehme, Nat. Commun. **3**, 898 (2012).
[24]P. A. Bobbert, T. D. Nguyen, F. W. A. van Oost, B. Koopmans, and M. Wohlgenannt, Phys. Rev. Lett. **99**, 216801 (2007).
[25]S. M. Sze, *Physics of Semiconductor Devices*, 3rd ed. (Wiley, New York, 2006).
[26]G. Horowitz, Adv. Mater. **10**, 365 (1998).
[27]V. F. Motsnyi, P. Van Dorpe, W. Van Roy, E. Goovaerts, V. I. Safarov, G. Borghs, and J. De Boeck, Phys. Rev. B **68**, 245319 (2003).
[28]A. Riminucci, M. Prezioso, C. Pernechele, P. Graziosi, I. Bergenti, R. Cecchini, M. Calbucci, M. Solzi, and V. A. Dediu, Appl. Phys. Lett. **102**, 092407 (2013).
[29]M. Ziese, I. Vrejoiu, and D. Hesse, Appl. Phys. Lett. **97**, 052504 (2010).
[30]M. Nishikawa, E. Kita, T. Erata, and A. Tasaki, J. Magn. Magn. Mater. **126**, 303 (1993).
[31]T. Burkert, L. Nordström, O. Eriksson, and O. Heinonen, Phys. Rev. Lett. **93**, 027203 (2004).
[32]J. H. Oh, S. Liu, Z. Bao, R. Schmidt, and F. Würthner, Appl. Phys. Lett. **91**, 212107 (2007).
[33]I. Bergenti, V. Dediu, E. Arisi, T. Mertelj, M. Murgia, A. Riminucci, G. Ruani, M. Solzi, and C. Taliani, Org. Electron. **5**, 309 (2004).
[34]H. Vinzelberg, J. Schumann, D. Elefant, R. B. Gangineni, J. Thomas, and B. Buechner, J. Appl. Phys. **103**, 093720 (2008).
[35]S. Majumdar, R. Laiho, P. Laukkanen, I. Väyrynen, H. Majumdar, and R. Österbacka, Appl. Phys. Lett. **89**, 122114 (2006).
[36]F. J. Wang, C. G. Yang, Z. V. Vardeny, and X. G. Li, Phys. Rev. B **75**, 245324 (2007).
[37]T. Francis, O. Mermer, G. Veeraraghavan, and M. Wohlgenannt, New J. Phys. **6**, 185 (2004).
[38]C. Barraud, P. Seneor, R. Mattana, S. Fusil, K. Bouzehouane, C. Deranlot, P. Graziosi, L. Hueso, I. Bergenti, V. Dediu, F. Petroff, and A. Fert, Nat. Phys. **6**, 615 (2010).
[39]D. Rabson, B. Jonsson-Akerman, A. Romero, R. Escudero, C. Leighton, S. Kim, and I. Schuller, J. Appl. Phys. **89**, 2786 (2001).
[40]R. Lin, F. Wang, J. Rybicki, M. Wohlgenannt, and K. A. Hutchinson, Phys. Rev. B **81**, 195214 (2010).
[41]C. Gould, C. Rüster, T. Jungwirth, E. Girgis, G. M. Schott, R. Giraud, K. Brunner, G. Schmidt, and L. W. Molenkamp, Phys. Rev. Lett. **93**, 117203 (2004).